Earthquakes and Structures, *Vol. 9, No. 6 (2015) 1193-1219*
DOI: http://dx.doi.org/10.12989/eas.2015.9.6.1193

Seismic performance of a 10-story RC box-type wall building structure

Kyung Ran Hwang[a] and Han Seon Lee[*]

School of Civil, Environmental, and Architectural Engineering, Korea University, Seoul, 136-713, Republic of Korea

(Received February 13, 2015, Revised July 2, 2015, Accepted October 7, 2015)

Abstract. The purpose of this study is to evaluate the seismic performance of high-rise reinforced concrete (RC) box-type wall structures commonly used for most residential buildings in Korea. For this purpose, an analytical model was calibrated with the results of the earthquake simulation tests on a 1:5 scale 10-story distorted model. This calibrated model was then transformed to a true model. The performance of the true model in terms of the stiffness, strength, and damage distribution through inelastic energy dissipation was observed with reference to the earthquake simulation test results. The model showed high overstrength factors ranging from 3 to 4. The existence of slab in this box-type wall system changed the main resistance mode in the wall from bending moment to tension/compression coupled moment through membrane actions, and increased the overall resistance capacity by about 25~35%, in comparison with the common design practice of neglecting the slab's existence. The flexibility of foundation, which is also commonly neglected in the engineering design, contributes to 30~50% of the roof drift in the stiff direction containing many walls. The possibility of concrete spalling and reinforcement buckling and fracture under the maximum considered earthquake (MCE) in Korea appears to be very low when compared with the case of the 2010 Concepcion, Chile earthquake.

Keywords: reinforced concrete; earthquake simulation test; wall; slab; membrane action

1. Introduction

The number of apartment dwelling units (8,576,000) comprises more than 58.4% of the total number (14,677,000) in Korea (KNSO 2010). These residential apartment buildings, as shown in Fig. 1, generally consist of high-rise reinforced concrete (RC) wall structures, and should be designed and constructed to resist earthquakes according to Korean building code, KBC 2005 (AIK 2005), which is similar to IBC 2000 (ICC 2000). Existing buildings not satisfying these codes should be evaluated and retrofitted. These high-rise box-type wall structural systems are defined as a bearing wall system in KBC 2005 or IBC 2000, but the style of these RC structures is unique in the world and the seismic performance of these structures has not been intensively investigated, neither in Korea nor abroad, except for a few studies.

*Corresponding author, Professor, E-mail: hslee@korea.ac.kr
[a]Ph.D. student, E-mail: dh8149@korea.ac.kr

http://www.techno-press.org/journals/eas&subpage=7 ISSN: 2092-7614 (Print), 2092-7622 (Online)

During the 2010 Chile earthquake (M_W 8.8), damage was generally concentrated in newer and taller buildings. In the typical construction of these Chilean RC wall buildings, the ratio of the total wall area to the floor plan area is on average roughly 3% in each principal direction of a building, with an average wall thickness of 15 cm to 20 cm (Wallace *et al*. 2012). In some sense, these structural properties are similar to those in Korea. The damage of the RC wall buildings was widespread and significant, and did not follow the failure mode typically assumed in design. The main observed damage to slender walls was concrete spalling in unconfined boundary elements and buckling and fracture of the reinforcement with horizontal cracks over almost the entire length of the wall due to high levels of axial load, as shown in Fig. 2(a) (Massone *et al*. 2012, Wallace *et al*. 2012). The wall boundary regions had relatively large spacing of horizontal web reinforcement, 20cm, with 90-degree hooks. Once cover concrete spalls in the inadequate boundary region subjected to large cyclic axial forces, the 90-degree hooks became ineffective and the concrete spalling contributed to buckling and fracture of vertical reinforcement in Fig. 2(b) (Wallace *et al*. 2012). This damage mode was also found in the 2011 Christchurch earthquake. The effects of the high vertical acceleration of the 2011 Christchurch earthquake could have also amplified the compression force demand on RC walls with already non-negligible axial load (Kam and Pampanin 2011).

Fig. 1 RC residential buildings in Korea: a bird's eye view of a district of Seoul

(a) Overall damage in the first-story shear walls (b) Fracture and buckling of reinforcement in the wall

Fig. 2 Damage of an RC wall building in the 2010 Chile earthquake (Wallace *et al*. 2012)

To identify the potential reasons for collapse of the 15-story wall-type, Torre Alto Rio residential building in Concepcion, under the 2010 Chile earthquake, Tuna and Wallace (2014) carried out static and dynamic response analyses of the nonlinear finite element model of a representative slice of the building, which included wall setbacks, irregularities, actual reinforcement details, and slab coupling, by using PERFORM-3D (CSI 2011). Analytical results were generally consistent with the reported damage. In the analytical results, the compressive concrete and reinforcement strains rapidly reached very large values, exceeding 0.03 m/m, at the web boundary of the T-shaped wall cross section only about one-half (22 seconds) of the way through the long duration of the Concepcion ground motion. After this point, analytical results of the model became unreliable. This type of failure tends to be abrupt, extend significantly into the wall web, and produces significant lateral strength loss. Slab coupling across the corridor reduces drift demands at a given time, but is insufficient to limit wall damage. Moehle *et al*. (2010) performed axial load tests of two specimens representing special boundary elements to evaluate the tensioning effect of a boundary element of thin walls on buckling failure. A boundary element, which was tensioned to 4% strain then compressed until failure, had a third of the compressive load capacity of the other specimen subjected to only compression. Although a more ductile failure was seen in the pre-tensioned case, the compression capacity was drastically decreased.

In the 1999 Turkey earthquake (M_W 7.4 Kocaeli), multi-story RC box-type wall buildings, constructed by using tunnel form techniques, were found to perform well under the earthquake. Balkaya and Kalkan (2003, 2004) investigated the seismic performance of the Turkish RC box-type building structures by conducting three-dimensional (3D) finite element pushover analysis to evaluate the influence of different plan configurations for different building heights. The interaction effect of slabs and transverse walls, which are perpendicular to the main walls and the loading direction, increased the overall capacity of the pierced shear walls despite the action of the door openings in strongly disrupting the shear flow between walls. Yuksel and Kalkan (2007, 2008) carried out experimental and analytical research on the seismic behavior of the box-type building using two 1:5 scale 4-story specimens under quasi-static cyclic lateral loading. The tension/compression coupling, which is executed by in-plane and membrane forces of the wall, caused brittle failure with fracture of longitudinal reinforcement in the outer walls. The failure occurred due to the low longitudinal reinforcement ratio of the walls. The minimum amount of longitudinal reinforcement was unable to carry the axial load, leading to cracking of concrete and the longitudinal reinforcement yielded and ruptured suddenly without warning.

Panagiotou *et al*. (2011) performed a shake table test (NEES-UCSD) of a full-scale 7-story building slice designed according to the displacement-based design procedure to observe the response of structures under unidirectional earthquake excitation. In the test representing the ASCE/SEI 7-05 (2006) design basis earthquake in southern California, spalling of the concrete cover in the special boundary elements of the first-story walls was observed, but longitudinal bar buckling did not occur. The confinement of boundary element provided excellent lateral stability to the longitudinal bars. In addition, three-dimensional interaction effects between the web wall, flange wall, and the slabs significantly increased the system overturning moment capacity as well as the shear force demand in the web wall. The coupling effect of the slab may be significantly greater in real buildings because the slabs were deliberately slotted in the sliced building specimen.

In accordance with the Canadian Standards Association (CSA), standards for the design of concrete structures, CSA-A23.3-04 (2004), coupled wall systems, which are classified as ductile, are divided into two different types for the purpose of determining a force modification factor, R_d. A ductile coupled shear wall system (R_d=4.0) has ductile shear walls connected by ductile coupling

beams where at least 66% of the base overturning moment resisted by the wall system is carried by axial tension and compression forces resulting from shear in the coupling beams. A ductile partially coupled wall system (R_d=3.5) has less stiff coupling beams such that less than 66% of the total base overturning moment is resisted.

For the structural design or analysis, the slabs are commonly assumed to be a rigid diaphragm, and the flexural stiffness of slabs is generally ignored. This assumption might be reasonable in frame systems. However, according to the study of Lee *et al*. (2002), slabs have a large influence on the lateral response of structure. Ignoring the flexural stiffness of slabs in the box-type RC building structures may lead to significant underestimation of the lateral stiffness of the structures. Therefore, they proposed an efficient method to analyze the box-type structures considering the effect of the slab using plate elements. In addition, information on the analytical model or method accounting for the effect of slab were suggested by Kunnath *et al*. (1991) and Wallace (2010). However, few analytical and experimental studies have focused on the effect of the slabs in the overall seismic performance of RC box-type wall building structures.

The purpose of this study is to evaluate the seismic performance of a 1:5 scale 10-story RC box-type wall building model based on analytical simulation by using the nonlinear analysis program, PERFORM-3D V5 (CSI 2011), which Lee et al. used to simulate the seismic response of shake-table tests on a 1:12 scale 17-story RC building structure with a high degree of torsional eccentricity and soft-story irregularities (2008) and the experimental results of cyclic reversed lateral force test on a two-story RC shear wall sub-assemblage (2012a). Both of the studies show reasonable analytical simulations. Therefore, firstly, PERFORM-3D was used to calibrate the analytical model with the results of the earthquake simulation tests on a 1:5 scale 10-story distorted model (Lee *et al*. 2012b). Secondly, the calibrated model was transformed to the true replica model. Then, the seismic performance of the true model in terms of the stiffness, strength, drift, and damage distribution was observed with reference to the earthquake simulation test results. General practice in design assumes a fixed base and neglects slabs in the lateral resistance, while the slab is designed only for gravity load. In this study, the effect of rigid foundations on the seismic performance was investigated by comparing the results from flexible-base (foundation rocking) and fixed-base models, and the effect of slabs was also observed by comparing the results from models with and without slabs as lateral resisting elements. In addition, since the results of earthquake simulation tests and analyses did not show the collapse, the behavior of the model under a more severe earthquake ground motion such as Concepcion, Chile earthquake in 2010, was observed, and nonlinear static pushover analysis was conducted to identify the collapse mode and ultimate capacity of the model.

2. Design of model and experimental setup

2.1 Design and construction of the experimental model

The prototype for the experiment was chosen to represent the most typical design in Korea. The floor area of one dwelling unit is 89 m^2 and one story accommodates two dwelling units, with 10 stories, as shown in Fig. 3. Though the prototype was designed according to the old design code of Korea, AIK 2000, this model will be evaluated based on the new seismic design code KBC 2005, which is similar to IBC 2000. In Eqs. (1) to (3), the design base shear, base shear coefficient, and fundamental period are estimated according to KBC 2005. Though the structural system in both the X and Y directions is assumed to be the bearing wall system with the use of R-factor, 4.5, the

natural period in the X direction was estimated by assuming a RC moment frame with that in the Y-direction obtained by using the equation for "other structures". Because the area of the walls in the X-directional frames is nearly 40% of that in the Y-directional frames, the X-directional periods obtained by using "other structures" could be considerably underestimated.

$$V=C_sW=1{,}530 \text{ kN (X-dir.) and } 2{,}300 \text{ kN (Y-dir.)} \tag{1}$$

$$C_S = \frac{S_{D1}}{(R/I_E)T_a} = 0.072 \text{ (X-dir.) and } 0.108 \text{ (Y-dir.)} \le \frac{S_{DS}}{R/I_E} = 0.117 \tag{2}$$

$$T_a=C_t(h_n)^{3/4}=0.865 \text{ sec (X-dir.) and } 0.580 \text{ sec (Y-dir.)} \tag{3}$$

where, V: base shear, C_s: base shear coefficient, W: weight, S_{D1}, S_{DS}: spectral accelerations at period 1 sec and 0.2 sec, respectively (0.234, 0.439), R: response modification factor (4.5), I_E: importance factor (1.2), T_a: fundamental period, C_t=0.073 (X-dir.): RC moment resisting frame (MRF), C_t=0.049 (Y-dir.): other structures, and h_n: height of structure (27 m).

In the general design practice, a fixed base is assumed with the slab neglected in the lateral resistance, while the slab is designed only for gravity load. The maximum drift ($\delta_u=C_d\times\delta_e/I_E=3.33\delta_e$) was estimated by applying a displacement amplification factor (C_d) of 4 and an importance factor (I_E) of 1.2 to the elastic drift (δ_e) of the earthquake load V. The calculated maximum story drift is 12.4 mm (0.46%) in the 9th story in the X direction and 1.88 mm (0.07%) in the 8th story in the Y direction, and these values are within the allowable limit of story drift of 1.5%.

The wall thickness is 180 mm or 160 mm and the slab thickness is 200mm. The ratio of wall cross sectional area to building floor plan area, A_w/A_f, is 2.67% and 4.71% in the X and Y directions, respectively. The reinforcement of the walls is two-layered and the steel ratio of the vertical reinforcement ranges from 0.34% to 0.90%, while the horizontal steel ratio is 0.29%.

Considering the capacity of the available shaking table (5 m×5 m) and the feasibility of model reinforcements, a 1:5 scale 10-story building model was chosen. The dead load, including the self-weight of the prototype model was 21,268 kN (unit floor dead load: 10.95 kN/m^2), and the weight of the 1:5 scale true replica model was estimated to be W_{total}=851 kN (self-weight, W_{self} = 145kN and added weight, W_{added}=706 kN). However, because this weight exceeds the maximum pay-load capacity of the shaking table, 600 kN, it was reduced again by half, W_{total}=425 kN (W_{self}=145 kN and W_{added}=280 kN), and acceleration was doubled by adopting the distorted model according to the Table 1. Dimensions of the experimental model are given in Figs. 4(a) to 4(c) with reinforcement details in Figs. 4(d) to 4(f).

Since it was difficult to make the cross sections of the model reinforcement conform exactly to the similitude law, the yield forces rather than yield stresses, were selected as the target (Lee and Woo, 1998). The model reinforcements, D3 and ϕ2, representing the D13 and D10 reinforcements with the nominal yield strength of 400 MPa in the prototype, are shown in Fig. 5(a). These model reinforcements were heat treated in a vacuum furnace to obtain the target yield forces (D3: 1.99~2.58 kN, D2: 1.12~1.45 kN) in accordance with the similitude requirements, and the test results of the strain-force curve in tension are shown in Fig. 5(b). The model concrete was made using the maximum aggregate size of 4 mm and the average 28-day compressive strength of 80 cylinder specimens (50 mm×100 mm) was 25.3 MPa with the design compressive strength in the prototype being 24 MPa. Detailed information on the design and construction of the specimen is given in the reference (Lee *et al*. 2012b).

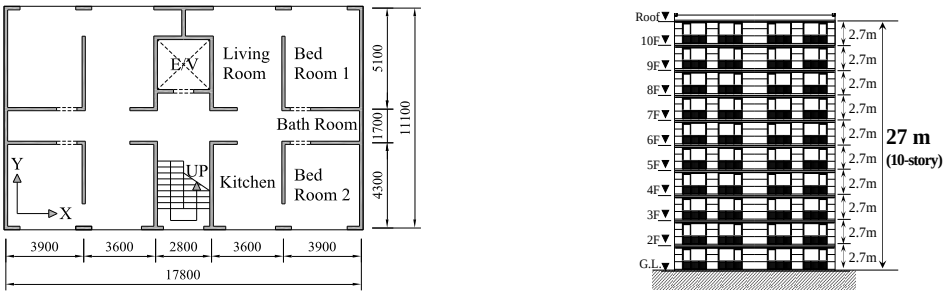

(a) Plan (b) Elevation

Fig. 3 Prototype building (unit: mm)

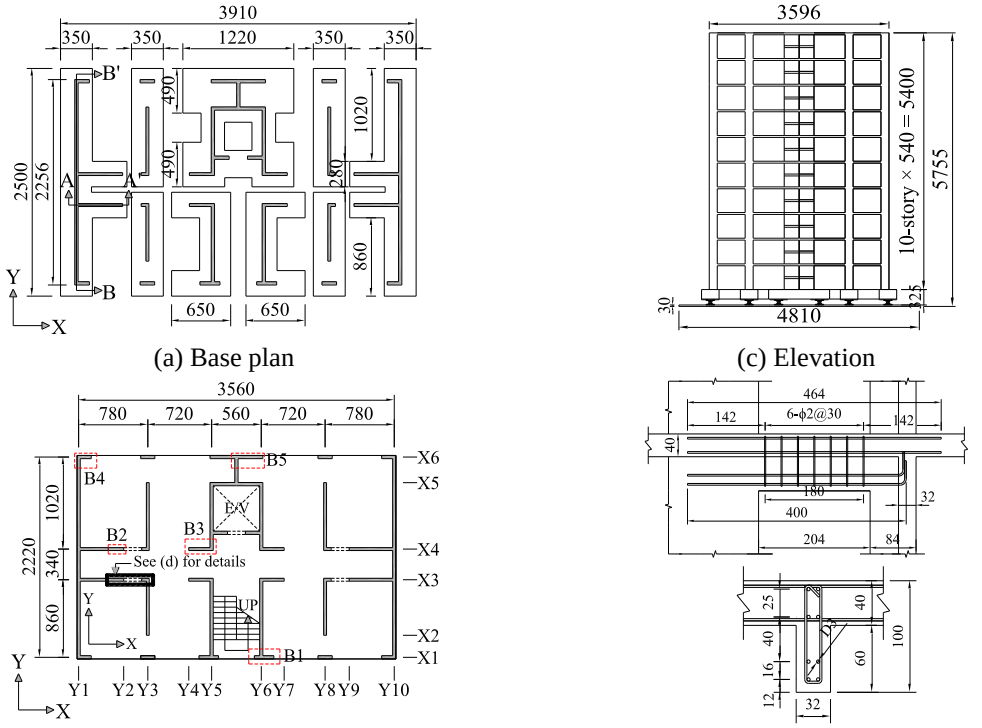

(b) Typical-floor plan (d) Details of the coupling beam

(e) Details of the wall (sections A-A' and B-B' in (a))

Fig. 4 Dimensions of 1/5 scale model (unit: mm)

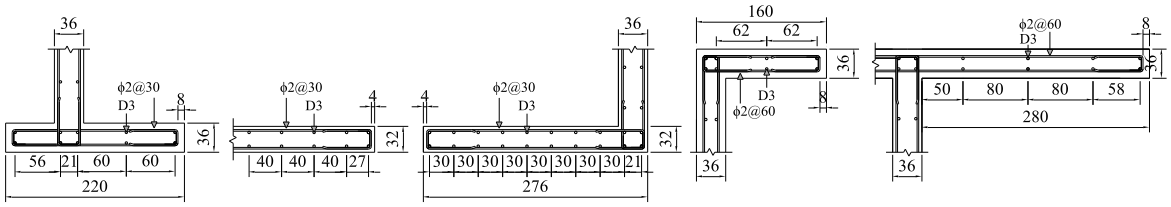

(f) Details of the boundary element in walls (B1 to B5 in (b))

Fig. 4 Continued

Table 1 Similitude law

Items	Dimension	True replica model	Distorted model	Items	Dimension	True replica model	Distorted model
Length	L	1/5	1/5	Velocity	LT^{-1}	$1/\sqrt{5}$	$1/\sqrt{(2/5)}$
Area	L^2	1/25	1/25	Acceleration	LT^{-2}	1	2
Density	M	1/5	1/10	Frequency	T^{-1}	$\sqrt{5}$	$\sqrt{10}$
(W_{total})		(851 kN)	(425 kN)	Time	T	$1/\sqrt{5}$	$1/\sqrt{10}$

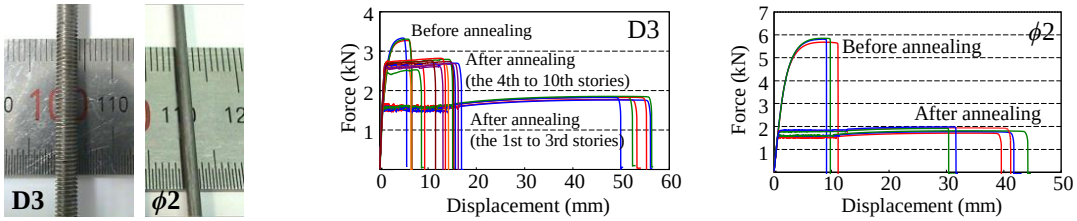

(a) D3 and $\phi 2$ (b) Typical force versus strain relation of D3 and $\phi 2$

Fig. 5 Model reinforcement D3 and $\phi 2$

2.2. Experimental setup, instrumentation, and test program

An overview of the experimental set-up is given in Fig. 6(a). The experimental set-up and instrumentation to measure displacements, accelerations, and forces are shown in Figs. 6(b) and 6(c). To measure lateral drifts and accelerations, displacement transducers and accelerometers were installed and the lateral drifts at the top and bottom of an independent post were measured at the corner of the shaking table to check the overturning movement of the shaking table itself, as shown in Fig. 6(b). Instrumentation to measure shear and flexural deformations was devised at the first and second stories. In addition, the normal strain distributions in the plastic hinge regions of the walls were measured. Displacement transducers (potentiometers) were installed to measure the flexural out-of-plane deformation of the slab. Load cells were installed beneath the footings to measure the two orthogonal directional shear forces and the axial force, as shown in Fig. 6(c).

The input accelerograms for earthquake simulations were based on the recorded 1952 Taft N21E (X direction) and Taft S69E (Y direction) components. Because the weight of the model was reduced to half of that of the true replica model considering the capacity of the shaking table, the input accelerogram was formulated by compressing the time axis with the scale factor of $1/\sqrt{10}$ and by amplifying the acceleration with the scale factor of two. Steel blocks shown in Fig. 6(b)

were attached to the model to compensate for the difference between the weight of model itself and that required, as per the similitude law (Table 1). The test program is given in Table 2. X, Y, and XY in the designation of each test mean that the excitations were implemented in the X direction only, in the Y direction only, and in the X and Y directions simultaneously, respectively.

Fig. 7(a) compares the design spectra as per KBC 2005 and response spectra obtained using the output accelerograms of shaking table excitations (Design Earthquake (DE): 0.187 g, Maximum Considered Earthquake (MCE): 0.3 g). The response spectra for the shake table output corresponding to DE and MCE simulate well the design spectra. Fig. 7(b) compares the design spectra and the base shear (or seismic) coefficients obtained through earthquake simulation tests. The values of seismic coefficients of the model under DE (0.187 g) are 0.15 and 0.18 in the X and Y directions, respectively.

(a) Overview of the experimental setup

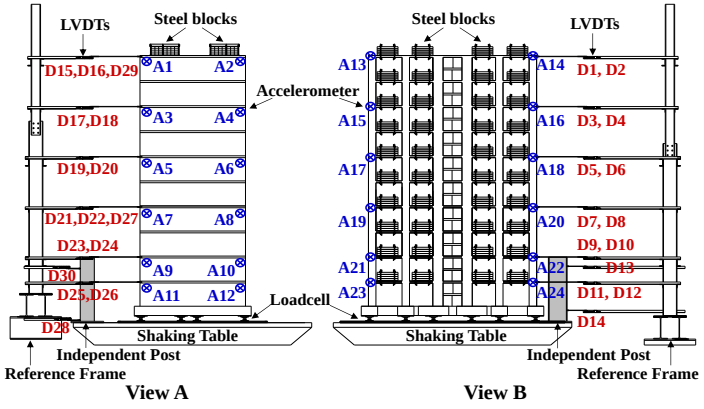

(b) Displacement transducers and accelerometers

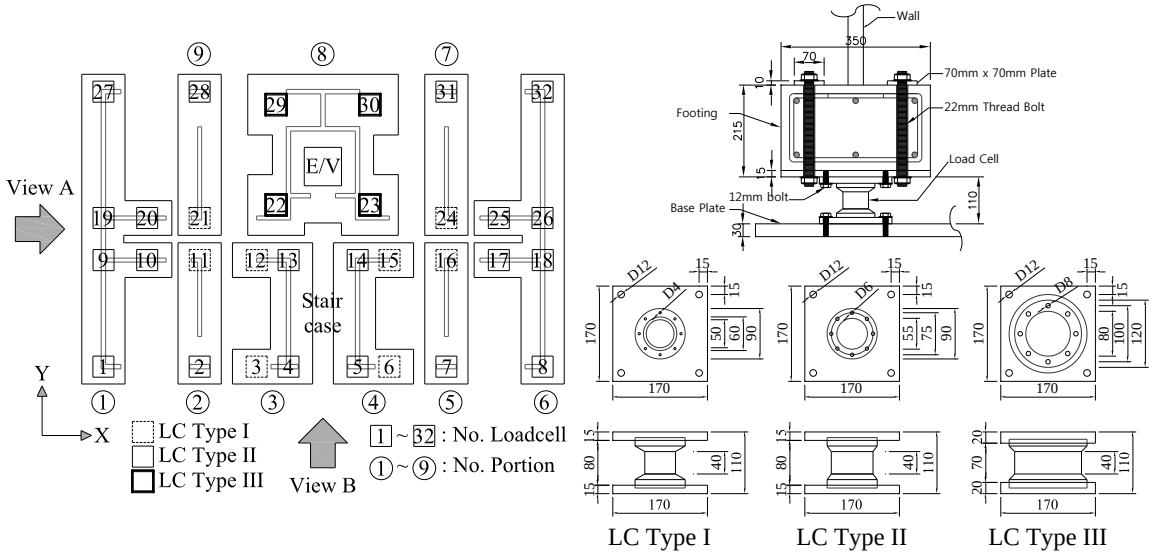

(c) Footings and load cells at base (unit: mm)

Fig. 6 Instrumentations

Table 2 Test program (X-dir.: 1952 Taft N21E, Y-dir.: 1952 Taft S69E)

Test	Intended PGA (g) (True replica model)		Input PGA (g) (Distorted model)		Output PGA (g) (Distorted model)		Return Periods in Korea (years)
	X-dir.	Y-dir.	X-dir.	Y-dir.	X-dir.	Y-dir.	
0.0175XY	0.0175	0.02	0.035	0.040	0.070	0.070	
0.035X	0.035	–	0.070	–	0.089	–	
0.035Y	–	0.04	–	0.080	–	0.104	
0.035XY	0.035	0.04	0.070	0.080	0.068	0.110	
0.07X	0.07	–	0.140	–	0.172	–	
0.07Y	–	0.0805	–	0.161	–	0.152	50 (Serviceability Level EQ., SLE)
0.07XY	0.07	0.0805	0.140	0.161	0.137	0.142	
0.154X	0.154	–	0.308	–	0.275	–	500
0.154XY	0.154	0.176	0.308	0.352	0.237	0.311	
0.187X	0.187	–	0.374	–	0.292	–	Design EQ. (DE)
0.187XY	0.187	0.216	0.374	0.431	0.316	0.450	
0.3X	0.3	–	0.60	–	0.523	–	2400 (Maximum Considered EQ., MCE)
0.3XY	0.3	0.346	0.60	0.691	0.525	0.643	

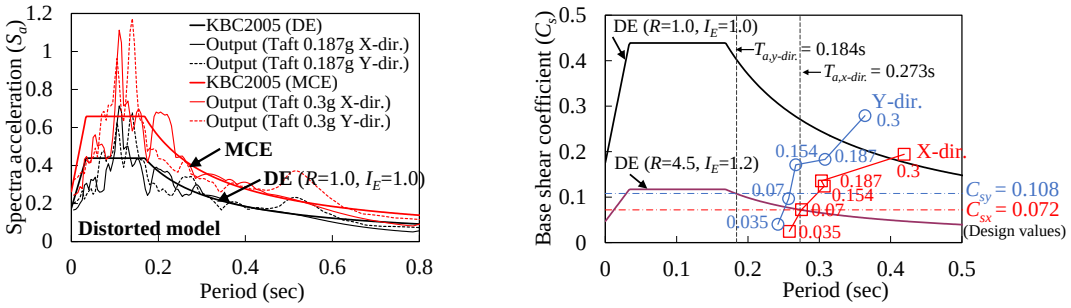

(a) Design and shake-table response spectra (b) Test results with the design spectra

Fig. 7 KBC 2005 design spectra and shake-table response spectra for the distorted model

3. Analytical modeling

This study presents the result of analytical simulation of shake-table responses of a 1:5 scale 10-story RC residential building model by using the nonlinear analysis program, PERFORM-3D (Computers and Structures, Inc. 2006). The relationships between stress and strain for concrete and steel are given in Figs. 8(a) and 8(b). The material model of concrete (Fig. 8a) is the Thorenfeldt model, which describes the spalling behavior of the concrete material with a nonlinear inelastic relationship. The tensile strength of concrete is assumed to be negligible. Since the envelope curve provided in PERFORM-3D cannot accept this model directly, the concrete curve is approximated with the tri-linear line. Fig. 8(b) shows the material models of reinforced bars, ϕ2 and D3. Specific material properties of concrete and reinforcement obtained in experiment are applied in the analyses. The backbone relation between shear strain and stress for the concrete shear of wall is given in Fig. 8(c). The shear backbone curve according to ASCE/SEI 41-13 (2014) is denoted by

dotted lines and the adjusted curve to fit the experimental results, which are the shear deformations of walls in the 1st and 2nd stories, is shown with solid lines.

Walls are modeled as inelastic "Shear Wall" element, which has 4 nodes and 24 degrees of freedom. In the longitudinal direction of the element, the axial and in-plane bending behaviors are described by using the inelastic fiber sections, as shown in Fig. 9(a), and the shear behavior is defined as the thickness of walls assigned to the inelastic concrete shear material in Fig. 8(c). Transverse in-plane bending is assumed to be elastic. Because PERFORM-3D provides only an elastic slab model, slabs are composed of the elastic beam elements with inelastic moment-curvature hinges at the ends of the beam obtained by inelastic sectional analyses, which describe the contribution of the slabs to the lateral strength of the building and the out-of-plane behaviors. The width of the slabs is determined depending on the availability of slab width, and the initial stiffness of the slab is 0.2*EI*. The "Shear Wall" element has no in-plane rotational stiffness at its nodes, so a very stiff beam element in the wall is modeled to specify a rigidly moment-resisting connection between the beam and wall. (CSI 2011) In addition, their diaphragm action for the rigid body motion is assumed. Coupling beams with details, as shown in Fig. 4(c), are modeled by using inelastic moment-curvature hinges at the ends of the beam and an inelastic shear hinge at the center of the beam. Because the length of the coupling beam is short, the coupling beam may yield in shear before yielding in flexure. The yield shear strength, V_p=10.2 kN, is assumed to be the sum of the yield strength by shear reinforcement, V_s=7.84 kN, and shear strength contributed by concrete, V_c=2.36 kN. To investigate the influence of the slab, the 10-story wall-type RC building without the slabs is also modeled. Model SB has both slabs and coupling beams, and Model NS has only coupling beams without slabs.

In order to take into account the influence of load cells beneath the footing in Fig. 6(c), footings and load cells are modeled as the elastic beam-column element. The result of shake table tests

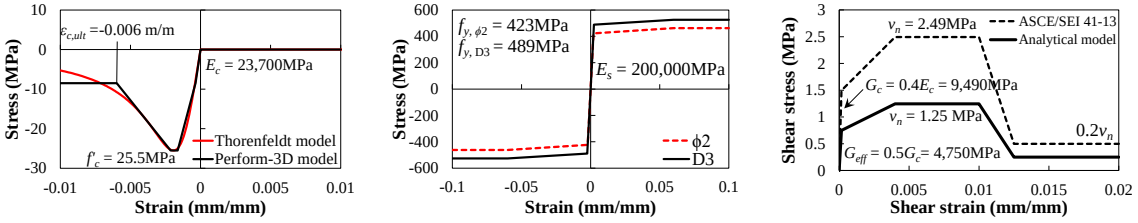

(a) Concrete (b) Steel (c) Shear material for wall

Fig. 8 Stress-strain relation of material

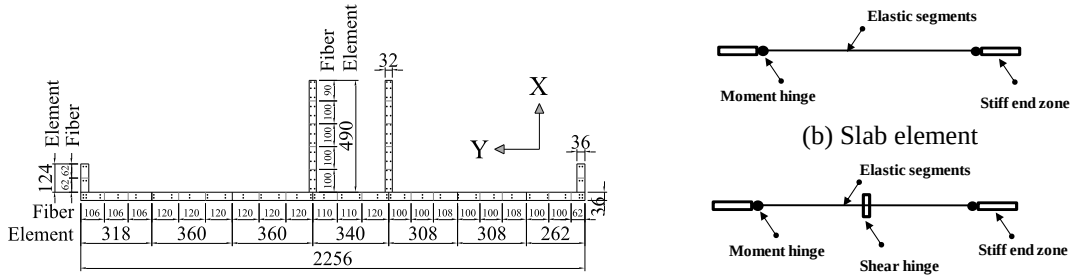

(a) Fiber section of the wall (unit: mm) (c) Coupling beam element

(b) Slab element

Fig. 9 Modeling details

shows that the load cells were not rigidly connected to the footing (flexible foundation), and observation of the videorecorded during the tests indicated the rocking behavior of the Y-directional outer walls as a rigid body. To reflect this phenomenon, the value of tensile stiffness is assumed to be half of those of compressive stiffness to simulate the tensile elongation, as shown in Table 3. The axial stiffness of the load cell was calibrated by matching the fundamental periods from the modal analysis to those derived from the test. The foundation rocking behavior could be well simulated by using the soil-structure interaction (SSI) model provided in ASCE 41-13 (2014). The structure-to-soil stiffness ratio, $h_{eff}/(V_sT)$, is used as a measure to determine whether SSI effects become significant, (NIST 2012), where, h_{eff} : the effective height of the building structure taken as approximately two-thirds of the building height (prototype: h_{eff}=18 m), V_s : the soil shear wave velocity, and T: the fixed-base building period (prototype: T_x=0.738 s and T_y=0.362 s). When the value of $h_{eff}/(V_sT)$ is larger than 0.1, the SSI effect is likely to be significant with lengthening of the building period. For the prototype building, the values of $h_{eff}/(V_sT)$ are 0.0488 and 0.0994 in the X- and Y-directions, respectively, assuming V_s=500 m/s for site class C, very dense soil and soft rock, in KBC 2005 (2005). Because the Y-directional ratio is close to 0.1, SSI effects are expected to occur. In ASCE/SEI 41-13 (2014), Winkler-style foundation spring model may be preferred, if the shallow foundation is rigid and axial load variations are important. The vertical stiffness of the SSI model for shallow rigid bearing footing (Fig. 10) based on Winkler-style foundation spring is suggested as follows

$$K_{end} = k_{end}\, l = \frac{6.83G}{1-\upsilon} l \quad \text{for B/6 end zones; and} \quad K_{mid} = k_{mid}\, l = \frac{0.73G}{1-\upsilon} l \quad \text{for middle zone} \tag{4}$$

$$G=\alpha G_0=\alpha v_s^2 \rho_s=317 \text{ MPa} \tag{5}$$

where, K_{end} and K_{mid}: vertical stiffness of the SSI model for end and middle zones, k_{end} and k_{mid}: the appropriate stiffness per unit length for end and middle zones, l: tributary length of footing, G: effective soil shear modulus (317 MPa), v: Poisson ratio (0.3 for sand), α: effective shear modulus ratio (0.622), G_0 : initial soil shear modulus (510 MPa), v_s: shear wave velocity at low strain at the approximate depth (500m/s), and ρ_s: soil mass density (20 kN/m^3/g for sand). The value of tensile stiffness at load cell no. 1 in Fig. 6(c), l,630 kN/mm (LC Type II), is comparable with that of the SSI model, 1,580 kN/mm (l=510 mm). In this study, both case of foundation rocking (flexible-base) and fixed (fixed-base) foundation are examined and compared in chapter 5.

An overview of the analytical model is given in Fig. 11. Gravity load analysis was conducted before conducting nonlinear static pushover analysis and nonlinear dynamic time history analysis. During 733 seconds (distorted model) and 1037 seconds (true replica model) of earthquake motion initiating from Taft 0.07 g and up to 0.6 g (distorted model) and from Taft 0.035 g and up to 0.3 g (true replica model), respectively, as shown in Table 2 and Figs. 12(a) and 12(b), the model was

Table 3 Axial stiffness of the elements for load cells

Type of load cell	Axial stiffness (kN/mm)		Allowable force (kN)	
	Tension	Compression	Axial	Shear
LC Type I	690	1380	203	41
LC Type II	1,630	3,260	480	98
LC Type III	5,030	10,060	1,476	303

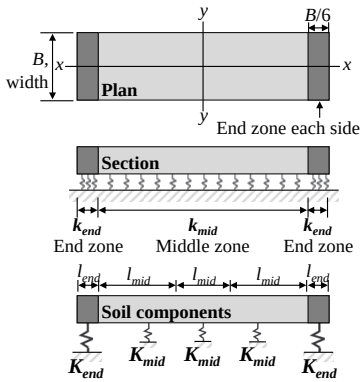

Fig. 10 Vertical stiffness modeling for shallow bearing footings (ASCE 41-13, 2014)

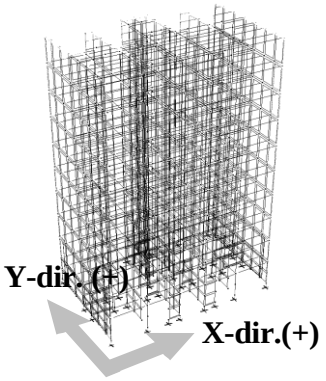

Fig. 11 Overview of the analytical model

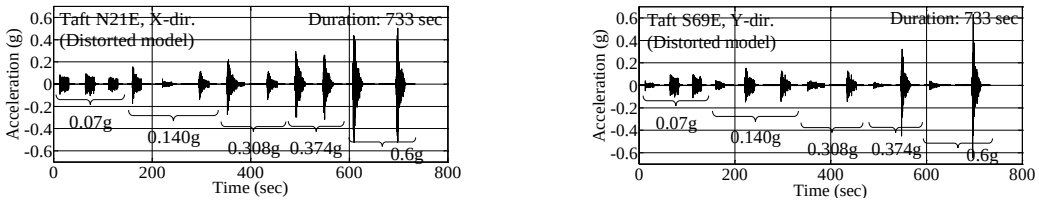

(a) 1952 Taft EQ. for the distorted model

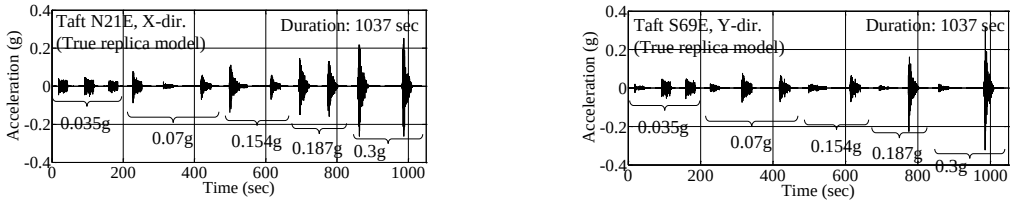

(b) 1952 Taft EQ. for the true replica model

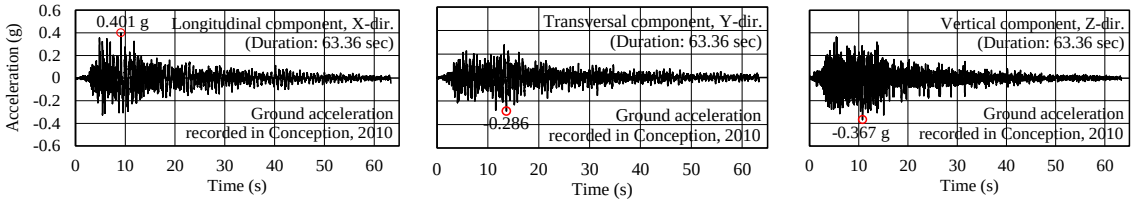

(c) 2010 Concepcion earthquake ground motion for the true replica model

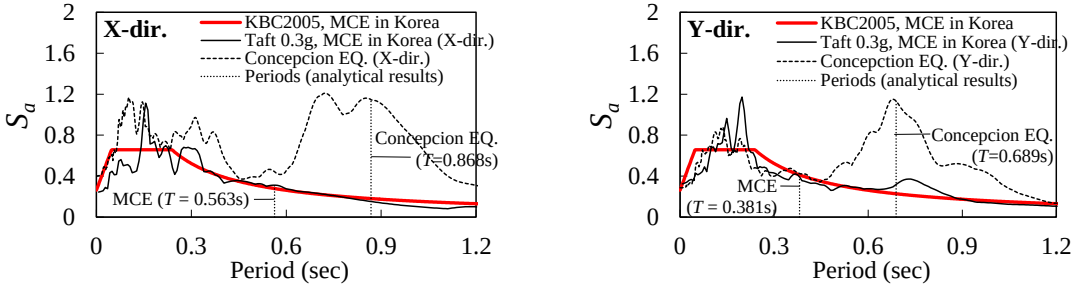

(d) Response spectra of MCE in Korea and 2010 Concepcion earthquake ground motion for the true replica model

Fig. 12 Recorded table excitations and response spectra used for analysis (See Table 2)

analyzed through the step-by-step procedure. Each base input excitation was the same as the output of the table motion in each test and separated with neighbor input sufficiently so that there would be no inertial forces when a new round of analysis was started. However, since the analysis is continuously conducted for the whole series of input motions, the damage caused by the preceding run could be taken into account in the subsequent run of analysis.

In addition, the analytical model was subjected to the longitudinal, transverse, and vertical components of the ground motion recorded in Concepcion, 2010 Mw 8.8 Chile earthquake (Fig. 12c) (Boroshek 2010). Elastic spectra of the 2010 Concepcion earthquake ground motion for 5% damping are shown in Fig. 12(d), along with the response spectra corresponding to MCE in Korea. The axis of period in the spectra is compressed by a scale factor of $1/\sqrt{5}$ for the true replica model. The response spectra of the Concepcion earthquake have in general much higher accelerations in the long-period region than the demand of MCE in Korea. Although a strong earthquake such as the Concepcion earthquake is considered unlikely to occur in the low-to-moderate seismicity region such as Korea, this study investigated the seismic performance of the model under the long-duration strong earthquake ground motion of the Concepcion earthquake.

Time steps are determined as 0.0039 s (distorted model) and 0.0055 s (true replica model) for the Taft earthquake and 0.00224 s (true replica model) for the Concepcion earthquake, and output is obtained for every two steps in order to avoid excessive amounts of data. Considering the damping effect in the time history analysis, the damping ratio of 4% at $0.652T_1$ ($=T_2$) and $1.0T_1$, where T_1 and T_2 are the first and second mode periods, respectively, was applied in using the Rayleigh model. The damping ratios, which were computed by the frequency response function analysis using roof acceleration outputs in results of the white noise test before the shake-table test, were 3.66% at the T_1 and 3.81% at the T_2.

4. Calibration of analytical model with experimental results

4.1 Calibration of analytical model

The experimental and analytical time histories of the base shear coefficient (base shear/building weight, V/W) and the roof drift in the X and Y directions under DE in Korea, 0.187XY, and MCE in Korea, 0.3XY, are compared in Fig. 13. The analytical model simulates well the time histories of the experiment.

The hysteretic curves between the base shear coefficient and the roof drift in the X- and Y-directions under 0.07XY (serviceability level earthquake; SLE), 0.187XY (DE), and 0.3XY (MCE) are given in Fig. 14. In the analytical results, the distorted model behaves linear elastically under 0.07XY, and the initial stiffness is comparable to that of the experiment. Under 0.187XY, a low level of inelastic response is revealed in the hysteresis between the base shear and the roof drift in X- and Y-directions. Significant inelastic behaviors were noticed in the hysteresis under 0.3XY. The analytical results of the distorted model generally simulate well the experimental results. However, in the hysteretic curve in the Y direction under 0.3XY, the energy dissipation and strength of the analytical model in the positive direction overestimate those of experimental results, whereas those in the negative direction are similar to those of the experimental results. In case of the true replica model, the X-directional behaviors are comparable to those of distorted model, but the maximum strength and the inelastic energy dissipation in the Y-directional behaviors under 0.3XY are 15% larger than those of distorted model. Nevertheless, in general the

differences between the true and distorted analytical models appear to be minor. *This paper presents only the seismic responses of the true replica model in the following analytical study.*

4.2 Evaluation of global behavior of structure

The experimental and analytical models possessed a large overstrength. Under MCE in Korea (0.3XY), the maximum values of *V/W* of the experiment and the analysis are 0.206 and 0.17 in the X direction, respectively, and 0.272 and 0.30 in the Y direction, respectively, which are 2.5~3.0 times larger than the design seismic coefficients, C_{sx}=0.072 and C_{sy}=0.108, respectively. Fig. 7(b) shows a significant increase of the base shear strength with the elongation of the fundamental periods in the inelastic response under the severe earthquakes. Elastic behavior was observed under 0.07XY, as shown in Fig. 14(a), with initial values of stiffness in experiment/analysis of 8.61 kN/mm/7.76 kN/mm in the X direction, and 18.3 kN/mm/17.7 kN/mm in the Y direction. Under 0.3XY in Fig. 14(c), the values of stiffness in experiment/analysis are 6.01 kN/mm/6.69 kN/mm in the X direction, and 14.4 kN/mm/15.3 kN/mm in the Y direction, which are 70%/57% of the initial stiffness in the X direction, and 84%/73% in the Y direction. Although the stiffness was reduced significantly and the amount of energy dissipation increased considerably, strength degradation was not observed.

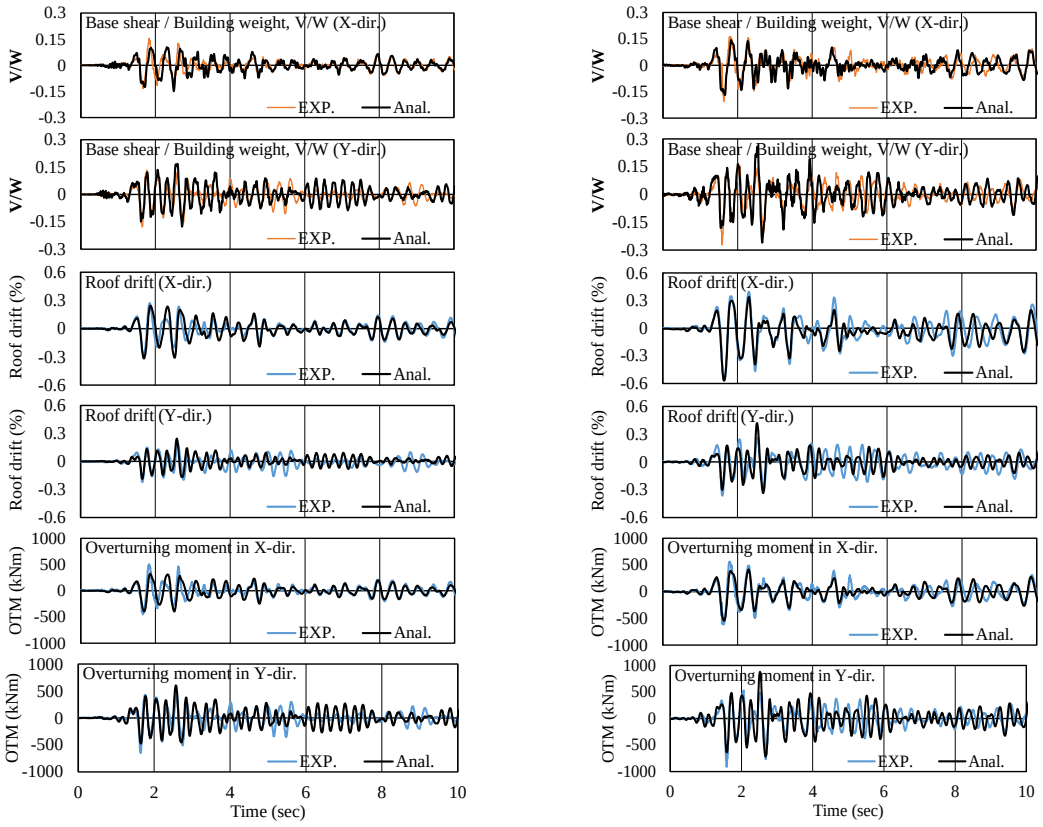

(a) 0.187XY (DE) (b) 0.3XY (MCE)

Fig. 13 Experimental and analytical relations of time histories of base shear, roof drift, and overturning moment (OTM)

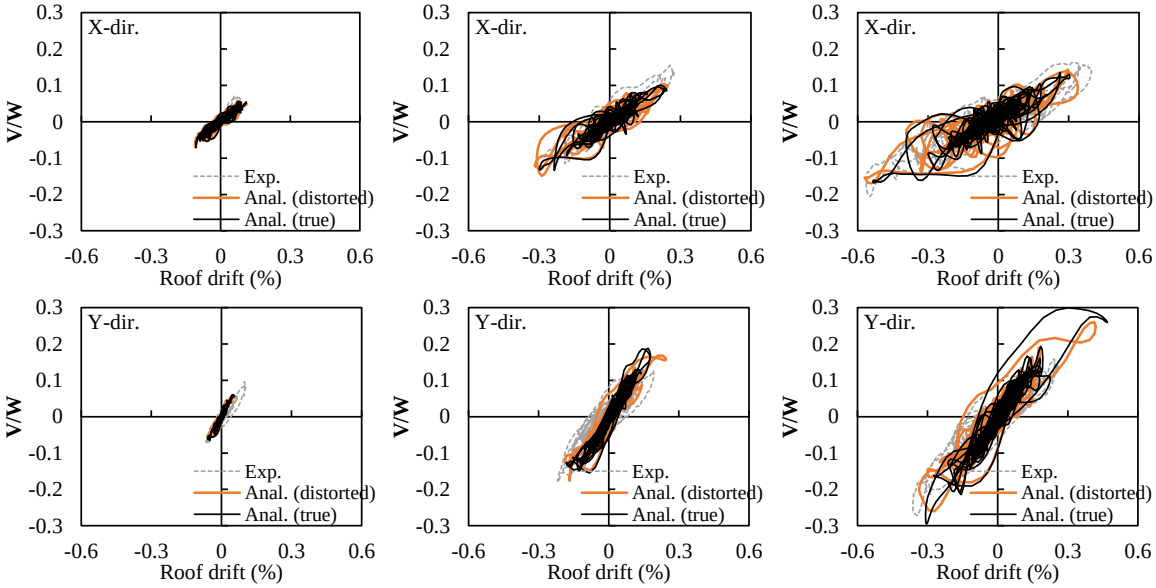

(a) 0.07XY (SLE) (b) 0.187XY (DE) (c) 0.3XY (MCE)

Fig. 14 Experimental and analytical relations of hysteretic curves between base shear and roof drift

Under DE in Korea (0.187XY), the maximum interstory drift ratio (IDR) in the analytical results is 0.33% in the 6th story in the X direction and 0.20% in the 7th story in the Y direction. These are comparable to those of the test results, 0.31% in the 5th to 6th stories in the X direction and 0.25% in the 9th to 10th stories in the Y direction, all of which satisfy the allowable IDR of 1.5% imposed by KBC 2005 (IBC 2000). In the elastic analysis for design, the calculated maximum IDR in the X direction, 0.46%, is approximately 30% overestimated, while the calculated IDR in the Y direction, 0.070%, is significantly underestimated with respect to the experiment and analysis under DE in Korea. This large discrepancy between the design and the experimental or simulated analytical drift ratio, particularly, in the Y direction, is attributed to the assumption of the fixed foundation in the design.

5. Effect of base flexibility of the building structure

Models with either the flexible base or fixed base were used to evaluate the effect of base flexibility (foundation rocking) on the seismic response of the building model. In Table 4, the flexible-base model has longer fundamental periods in the X- and Y directions by 24% and 43%, respectively, than the fixed-base model. The capacity curves with the flexible base and fixed base obtained from the static pushover analyses are compared in Fig. 15. The lateral load pattern is derived from the first modal shape. Limit states were defined for the strain of steel, concrete, and shear materials in Fig. 8 as follows: steel yielding at ε_y=0.002 m/m (circle marker), concrete compressive strength degradation at ε=0.002 m/m (hollow triangle marker), concrete ultimate compressive strain at $\varepsilon_{c,ult}$=0.006 m/m (solid triangle marker), and shear stress degradation in the wall at ε=0.01 m/m (rectangular marker), the corresponding points of which are given in Fig. 15.

Table 4 Natural periods obtained from modal analysis (unit: second)

True replica model	Mode	Model SB	Model NS
Flexible-base	1st (X-dir.)	0.433	0.552
	2nd (Y-dir.)	0.284	0.313
Fixed-base	1st (X-dir.)	0.330	0.388
	2nd (Y-dir.)	0.162	0.172

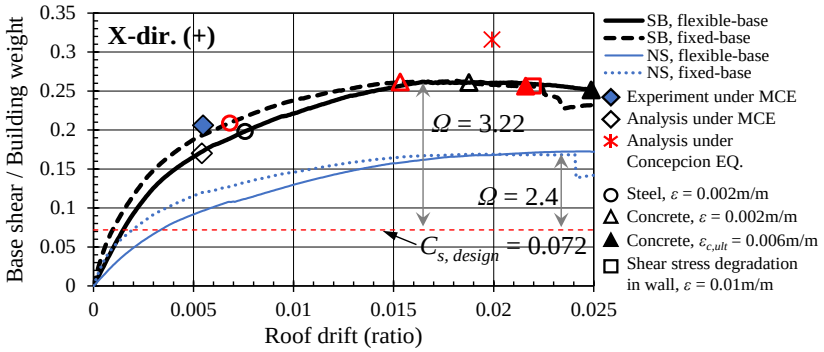

(a) X-dir.

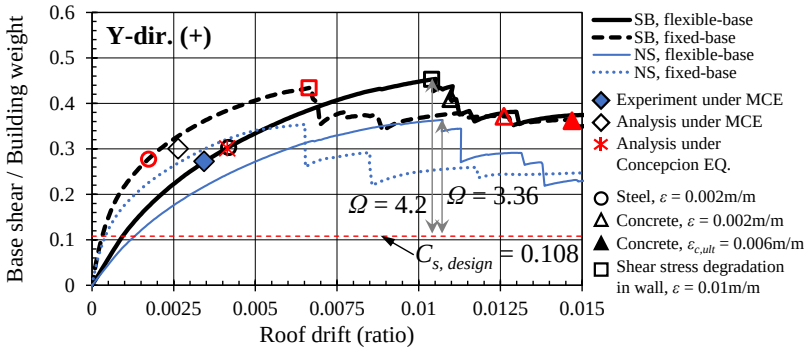

(b) Y-dir.

Fig. 15 Pushover (capacity) curves

In the X direction, the pushover curve with the flexible base indicates that the initial stiffness, 7.89 kN/mm, is half of that of the fixed-base model, 15.3 kN/mm, and that the base shear at 0.5% roof drift, 0.165*W*, is lower than that of the fixed-base model, 0.187*W*. However, the maximum lateral strengths of the flexible-base and fixed-base model in the X direction are equal to 0.232*W* at approximately 1.6% roof drift. In the Y direction, the initial stiffness of the flexible-base model, 18.5 kN/mm, was significantly lower than that of the fixed-base model, 62.7 kN/mm. The point of the peak resistance of the flexible-base model in the displacement was significantly delayed when compared with that of the fixed-base model. The maximum lateral strength of the fixed-base model in the Y direction, 0.434*W*, occurred at roof drift 0.67%, whereas that of the flexible-base model was 0.454*W* at the 1.05% roof drift. The lateral strength of the fixed-base and flexible-base models dropped suddenly after the point of the peak resistance (at roof drift 1.05% in the flexible-base model) due to the shear failure in the Y-directional outer walls.

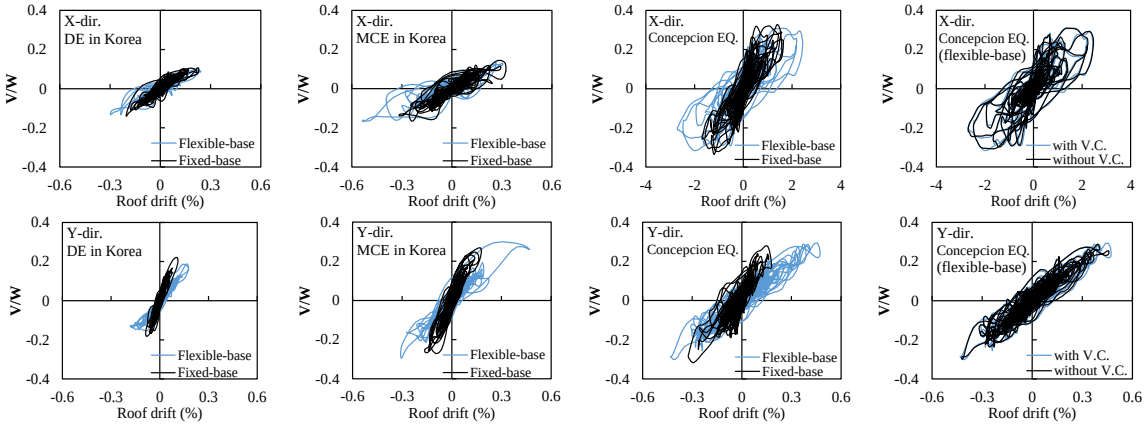

(a) Flexible-base vs. fixed bases models under DE in Korea

(b) Flexible-base vs. fixed bases models under MCE in Korea

(c) Flexible-base vs. fixed bases models under Concepcion EQ

(d) Concepcion EQ. with/without V.C.

Fig. 16 Hysteretic curves between base shear and roof drift

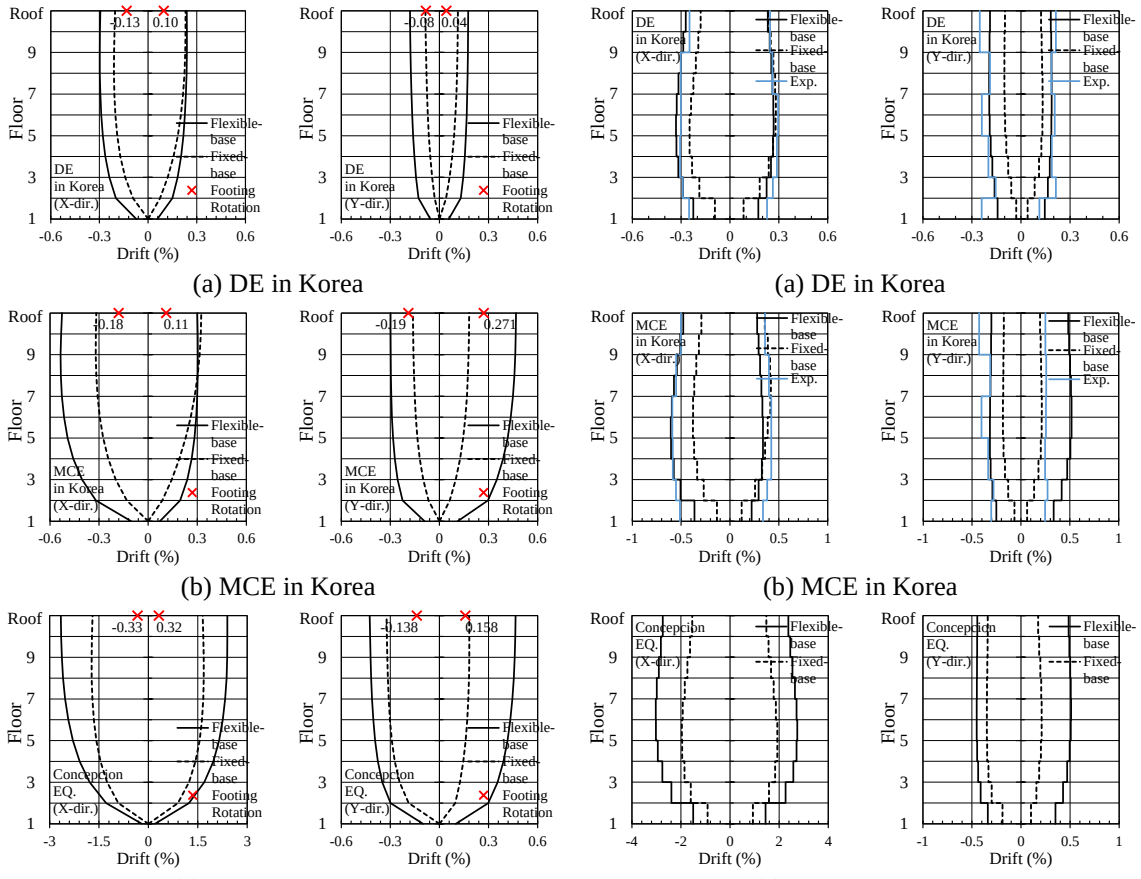

(a) DE in Korea

(b) MCE in Korea

(c) Concepcion EQ.

Fig. 17 Lateral drift ratio with respect to the base at the time instant of maximum roof drift

(a) DE in Korea

(b) MCE in Korea

(c) Concepcion EQ.

Fig. 18 Envelope of interstory drift

Results of the nonlinear time history analysis for the fixed-base model show quite different behavior from those for the flexible-base model as shown in Figs. 16(a), (b), and (c). The maximum roof drifts in the X- and Y directions of the fixed-base model are much smaller than those of the flexible-base model, whereas the maximum values of base shear in the X- and Y directions of the fixed-base model are similar to those of the flexible-base model. Fig. 16(d) compares the hysteretic curves between the base shear and the roof drift of the flexible-base model with and without the vertical component of ground motion in the Concepcion earthquake, which are very similar to each other and the influence of the vertical component of ground motion appears to be insignificant.

The lateral drift ratio with respect to the base at the time instant of the maximum roof drift and the envelope of IDR are presented in Figs. 17 and 18, in which all of the lateral drifts and interstory drifts in the flexible-base model are larger than those in the fixed-base model, except for the +X direction under MCE in Korea. Under MCE in Korea, the X- and Y-directional maximum roof drifts of the flexible-base model are 1.68 and 2.67 times, respectively, larger than those of the fixed-base model. The rocking behavior of the footing ("x" marker in Fig. 17) in the X- and Y directions contributes 33% and 56%, respectively, of the corresponding roof drifts with the contribution of the foundation rocking under the Concepcion earthquake being 13% (X-dir.) and 32% (Y-dir.), respectively. The translational behavior in the Y direction is more sensitive to the flexibility of foundation than that in the X direction. All of the interstory drifts in Fig. 18 are within 0.6% under MCE in Korea. However, the maximum interstory drifts in the X direction of the flexible-base and fixed-base model under the Concepcion earthquake are approximately 3% and 2%, respectively.

6. Effect of slabs on the lateral resistance

To investigate the influence of the slab on the earthquake resistance, the 10-story wall-type RC building without slabs is modeled. Model SB with slabs has been described already in section 3. The slab of Model NS is modeled by assuming the in-plane rigid diaphragm, but ignoring the flexural rigidity of the slab. Table 4 compares the natural periods of Models SB and NS with the flexible base obtained from modal analyses. The first-mode periods of Models SB and NS are 0.433 sec and 0.552 sec, respectively, for the translational mode in the X direction.

Fig. 15 compares the capacity curves of Models SB and NS with the flexible base obtained from pushover analyses in the X and Y directions. In the X direction (Fig. 15(a)), the initial stiffnesses of Models SB and NS are 7.89 kN/mm and 4.31 kN/mm, respectively. At the 0.5% roof drift, the X-directional base shear coefficient (base shear/building weight, V/W) of Model SB, 0.165, is also approximately two times larger than that of Model NS, 0.0912. In the Y direction (Fig. 15(b)), the initial stiffness and the base shear coefficient at the 0.5% roof drift of Model SB, 18.6kN/mm and 0.332, are about 1.3 times larger than those of Model NS, 14.4 kN/mm and 0.272, respectively. The overstrength factor of the model with slabs, Ω, which is defined as the ratio of the maximum strength of the fully-yielded system to the design seismic coefficients, is 3.22 and 4.2 in the X and Y directions, compared to 2.4 and 3.36 in the model without slabs, respectively. The strengths of the model with slab are 25~35% larger than those of that without slabs.

In Table 5, the influence of the existence of the slab on the X-directional overturning moment (OTM) is observed. The OTM is resisted by both the bending action and the coupling action due to the membrane forces of the walls. The base of footing is divided into nine portions, i=1 to 9, as

Table 5 Maximum overturning moment, OTM (unit: kNm)

		Table excitation	Total OTM ($\sum F_j h_j$)	OTM due to T/C coupling ($\sum P_i l_i$)	Degree of coupling ($\sum P_i l_i / \sum F_j h_j$)
Model SB	Flexible-base	Taft 0.07XY (SLE)	187	85.8	45.9%
		Taft 0.187XY (DE)	418	208	49.8%
		Taft 0.3XY (MCE)	561	272	48.5%
		Concepcion EQ.	1025	473	46.1%
	Fixed-base	Taft 0.07XY (SLE)	218	85.4	39.3%
		Taft 0.187XY	395	177	44.7%
		Taft 0.3XY (MCE)	494	247	50.1%
		Concepcion EQ.	910	402	44.1%
Model NS	Flexible-base	Taft 0.07XY (SLE)	155	31.6	20.4%
		Taft 0.187XY (DE)	293	59.2	20.2%
		Taft 0.3XY (MCE)	417	102	24.5%
		Concepcion EQ.	707	199	28.1%
	Fixed-base	Taft 0.07XY (SLE)	166	39.7	24.0%
		Taft 0.187XY (DE)	290	66.2	22.8%
		Taft 0.3XY (MCE)	393	119	30.3%
		Concepcion EQ.	669	163	24.3%

shown in Fig. 6(c). The external OTM, $\sum F_j h_j$, is resisted by the sum of the wall bending moments, $\sum M_i$, and the sum of the coupling moment due to the tension and compression (T/C) forces in the wall, $\sum P_i l_i$, as given by Eq. (6)

$$\sum F_j h_j = \sum M_i + \sum P_i l_i \tag{6}$$

$$\text{Degree of coupling (d.o.c)} = \frac{\sum P_i l_i}{\sum F_j h_j} \tag{7}$$

where, F_j is the external lateral force at the jth floor, h_j is the height of the model at the j story, M_i and P_i are the base bending moment and the axial force, respectively, at the portion i as defined in Fig. 6(c), and l_i is the distance of the portion i from the geometric center of the structure. Table 5 compares the X-directional resisting OTM due to the coupling, $\sum P_i l_i$, with the total OTM, $\sum F_j h_j$, of Models SB and NS at the time instant of the maximum OTM. Under MCE in Korea (Taft 0.3XY), the maximum OTM demands of Model SB with the flexible base are 561 kNm, which is about 1.3 times larger than those of Model NS, 417 kNm. In Model SB, the coupling moments are approximately 40 to 50% of the total OTM, with those in Model NS ranging from about 20 to 30%. Regardless of the flexibility of the base and the intensity of earthquake ground motions, the degree of coupling, $\sum P_i l_i / \sum F_j h_j$, remains almost unchanged.

7. Distribution of damage through inelastic behavior

The damage patterns in the slab and wall after all tests were completed are shown in Figs. 19 to 21. Fig. 19(a) shows the crack pattern on the roof and third-floor slab in the experimental model. Cracks were concentrated across the long-span slab and along the slab-wall joint in the Y direction. Most of the floors showed similar crack patterns to those of the third-floor slab. Fig. 19(b) demonstrates the overall view of the crack pattern on the bottom sides of slabs. The outer walls in the X and Y directions have many horizontal cracks penetrating almost the full length of the walls at the lower stories, as shown in Fig. 20. Fig. 21 shows the crack patterns of the inner walls, which are mainly flexural with minor shear cracks.

The damage patterns of the wall indicate that the walls were subjected to not only flexural bending but also in-plane membrane forces due to the three-dimensional interaction effect between the walls and slabs. The wall system with openings resists the OTM through axial tension and compression coupling forces leading to the membrane action in the wall. In particular, the outer walls, when the large lateral load acts in the perpendicular direction, behave as a flange wall and resist the large axial tension and compression forces, whereas the web walls act as bending elements. This leads to many horizontal cracks at the lower stories in the outer walls, as shown in Fig. 20. This experimental observation will be compared with the analytical results in the following.

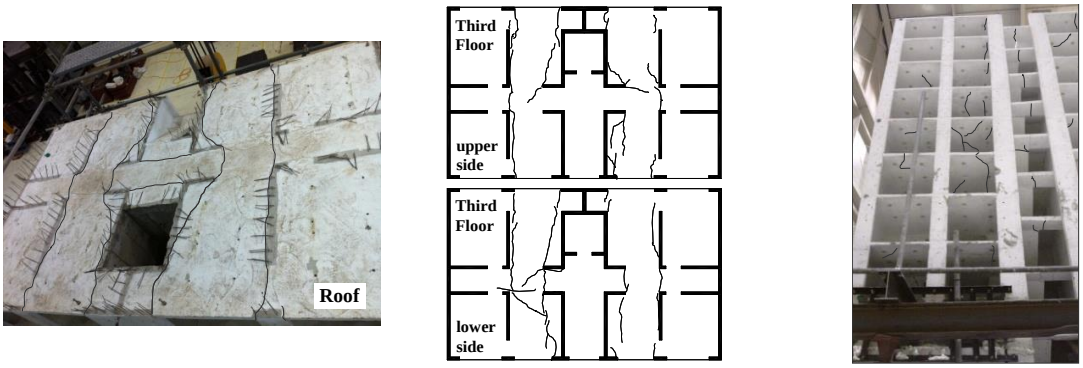

(a) view of the roof and 3rd floor slab (b) view to the undersides of slabs

Fig. 19 Crack patterns in slabs

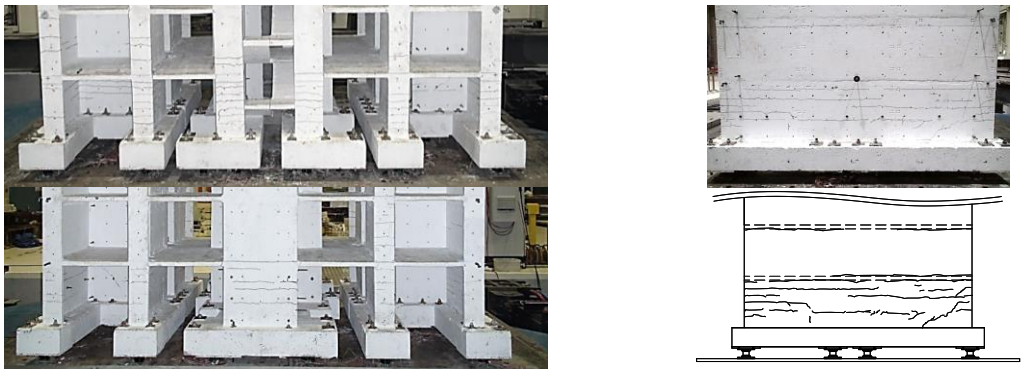

(a) Exterior walls in X-dir. (b) Exterior walls in Y-dir.

Fig. 20 Crack patterns in exterior walls


(a) View A


(b) View B


(c) View C


(d) View D


(e) View E

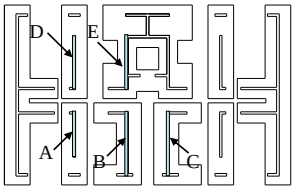

(f) View points

Fig. 21 Crack patterns in critical interior walls in the Y direction

The deflection shapes with the distribution of plastic hinges in the slabs and coupling beams for Frame X4 (Fig. 4(b)) at the time instant of the maximum roof drift in the negative X direction are shown in Fig. 22. The plastic moment hinges at the ends of the slab element are denoted by solid circles, and the shear plastic hinge at the center of the coupling beam element by hollow circles. In the flexible-base model under MCE in Korea (Fig. 22(a)), plastic moment hinges developed at almost all the ends of slab elements, and shear plastic hinges occurred all the coupling beam elements between Axes Y2 and Y3. In the fixed-base model (Fig. 22(b)), on the other hand, plastic moment hinges did not formed at some slab elements between Axes Y3 and Y4, and plastic shear hinges occurred at the center of all coupling beam elements. Under the Concepcion earthquake in both the flexible-base and the fixed-base models (Figs. 22(c) and 22(d)), the shear plastic hinges and the plastic moment hinges formed all over the structure.

In the hysteretic curves between the base shear and roof drift (Figs. 14 and 16), significant energy dissipation is observed under MCE in Korea (0.3XY) and the Concepcion earthquake. Fig. 23 depicts time histories of the total dissipated energy, and Table 6 compares the amount of dissipated energy in each element group. The amount of dissipated inelastic energy increases with increasing earthquake intensity.

In case of the flexible-base model, the amounts of the total dissipated inelastic energy under SLE, DE, and MCE in Korea are 53.9 kNmm, 839 kNmm, and 4,680 kNmm, respectively. In particular, the amount of the total dissipated energy under the Concepcion earthquake, 63,700 kNmm, is approximately 13.6 times larger than that under MCE in Korea. The amount of the dissipated energy during the maximum responses, 2 to 8 sec under DE and MCE in Korea and 6 to 15 sec under the Concepcion earthquake, covers over 80% of the total dissipated energy. Under SLE in Korea, over 90% of the total energy is dissipated by the coupling beam elements, whereas the ratio of the amounts of dissipated energy in the wall : slab : coupling beam is approximately 7:2:1 under MCE in Korea and the Concepcion earthquake.

The amount of the total dissipated energy in the fixed-base model is 20~40% larger than that in the flexible-base model. Under MCE in Korea and the Concepcion earthquake, the ratio of the amounts of dissipated inelastic energy in the wall : slab : coupling beam in the fixed-base model is about 8:1.2:0.8. The fixed-base model increases the dissipated inelastic energy in the wall, while

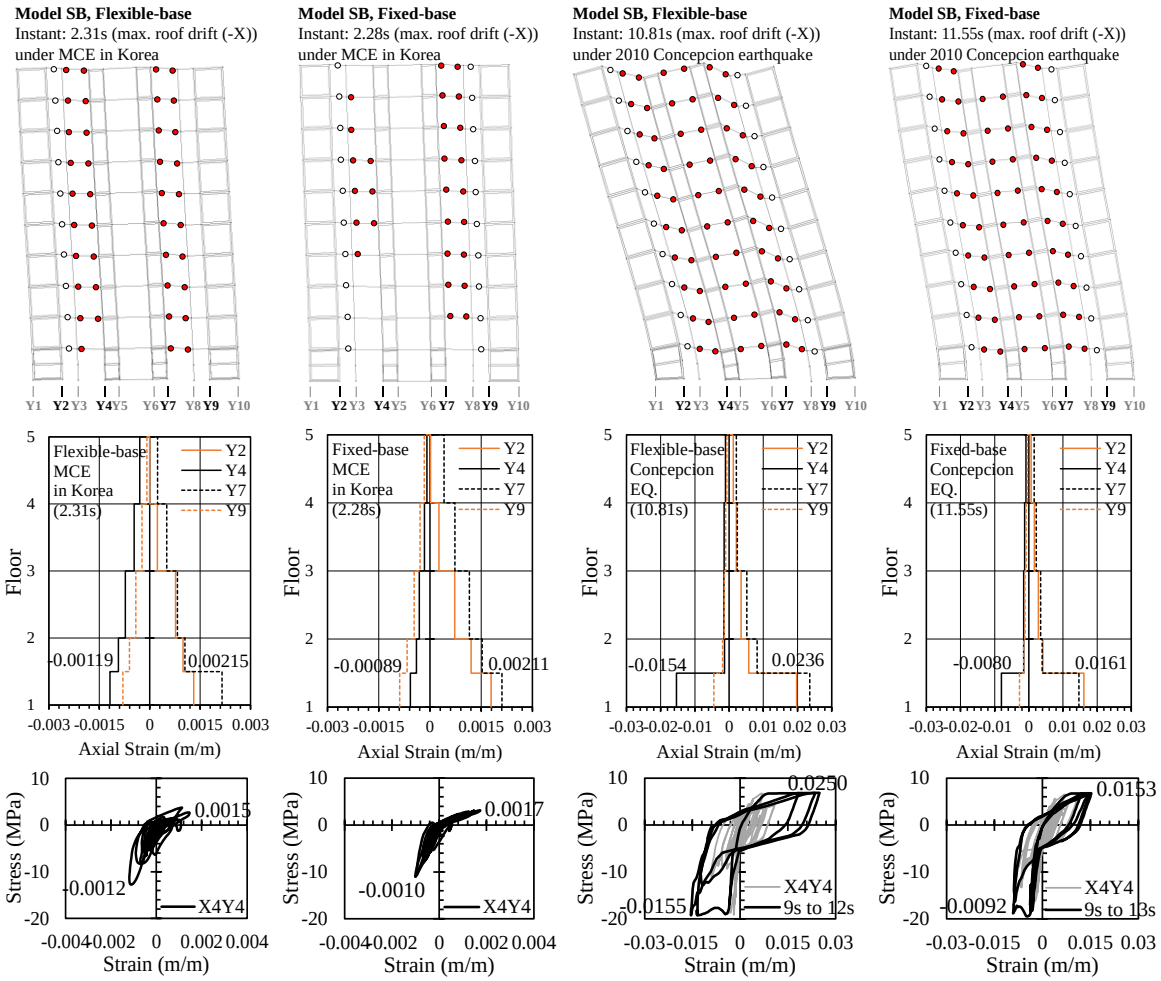

(a) Flexible-base model under MCE in Korea (b) Fixed-base model under MCE in Korea (c) Flexible-base model under Concepcion EQ. (d) Fixed-base model under Concepcion EQ.

Fig. 22 Distribution of plastic hinges and axial strain of inner walls in Frame X4 at the time instant of the maximum roof drift in the negative X direction

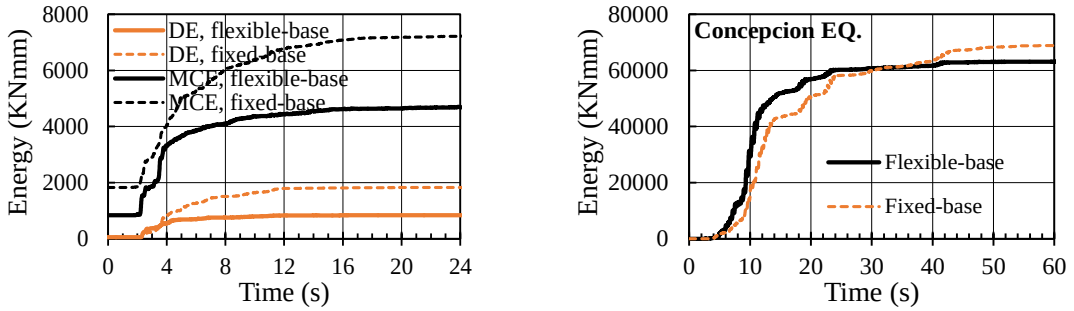

(a) True replica model under DE and MCE (b) True replica model under the Concepcion EQ.

Fig. 23 Dissipated inelastic energy

Table 6 Dissipated inelastic energy of element groups (unit: kNmm)

Model	Table excitation	Dissipated inelastic energy of element groups (unit: kNmm)			
		Wall	Slab	Coupling beam	Total
Flexible-base	Taft 0.07XY (SLE)	3.4 (6.4%)	0.8 (1.6%)	49.6 (92.1%)	53.9 (100%)
	Taft 0.187XY (DE)	462 (55.1%)	178 (21.2%)	198 (23.7%)	839 (100%)
	Taft 0.3XY (MCE)	3300 (70.5%)	883 (18.9%)	500 (10.7%)	4680 (100%)
	Concepcion EQ.	44300 (69.6%)	13300 (20.8%)	6110 (9.6%)	63700 (100%)
Fixed-base	Taft 0.07XY (SLE)	4.4 (7.9%)	0.0 (0.0%)	51.6 (92.1%)	56.0 (100%)
	Taft 0.187XY (DE)	1390 (76.0%)	46.5 (2.5%)	392 (21.5%)	1829 (100%)
	Taft 0.3XY (MCE)	6120 (84.7%)	335 (4.6%)	770 (10.7%)	7220 (100%)
	Concepcion EQ.	55900 (80.5%)	8260 (11.9%)	5290 (7.6%)	69400 (100%)

decreasing that in the slab and coupling beam, when compared with the case of the flexible-base model. Under MCE in Korea, the amount of the inelastic energy dissipated by the wall in the fixed-base model, 6120 kNmm, is significantly larger than that in the flexible-base model, 3300 kNmm, but the amount of the inelastic energy dissipated by the slab in the fixed-base model, 335 kNmm, is less than that in the flexible-base model, 883 kNmm.

8. Axial strain demand in wall

In Figs. 20 and 21, the walls have many horizontal cracks at the lower stories due to the large membrane forces. To assess the demand in tensile and compressive strain, the axial strains at various locations are measured by using "Gage" elements in PERFORM-3D, which are fictitious without any effect on the structural behavior.

Fig. 22 shows the vertical distributions of the axial strain for wall boundaries in the locations Y2, Y4, Y7, and Y9 for Frame X4 (Fig. 4(b)) at the time instant of the maximum roof drift in the -X direction. The maximum tensile and compressive strains occurred at the boundaries of the core wall in the locations Y4 and Y7, respectively, at the base of the building. In the lowest parts of Fig. 22, the axial stress-strain hysteretic responses in the part of core wall, the location X4Y4, under MCE in Korea reveal a small amount of energy dissipation, whereas those under the Concepcion earthquake show significant inelastic behaviors, not only on the tension side but also on the compression side. In these hysteretic responses under the Concepcion earthquake, significant compressive stress degradation occurred during the time span from 9 s to 12 s (flexible-base) and from 9 s to 13 s (fixed-base), due to the loss of concrete strength. In other words, the compressive behavior of this part did not coincide with that of the material model for concrete in Fig. 8(a), but was governed by the material model for steel in Fig. 8(b) after reaching the ultimate strength of the concrete at approximately 0.003 m/m.

Table 7 compares the maximum axial strain demands at wall boundaries 3, 4, and 5, as shown in Figs. 4(b) and 4(f). Boundary 3 is in the core wall at the location Y4 in the Frame X4, and boundaries 4 and 5 are located in the X- and Y-directional outer walls, respectively. Under MCE in Korea, the maximum tensile and compressive strains are 0.00528 m/m at boundary 4 and 0.00119 m/m at boundary 3, respectively. The tensile strains at the outer wall exceed the yield

Table 7 Maximum axial strain demand of the wall boundaries (unit: m/m, Fig. 4b)

Model	Table excitation	T/C strain	Maximum axial strain demand at critical locations of the wall		
			B3 (X4Y4)	B4 (X6Y1)	B5 (X6Y6)
Flexible-base	Taft 0.3XY (MCE)	Tension	0.00147	0.00528	0.00381
		Compression	0.00119	0.00090	0.00077
	Concepcion EQ.	Tension	0.0250	0.0128	0.0252
		Compression	0.0155	0.00108	0.00688
Fixed-base	Taft 0.3XY (MCE)	Tension	0.00174	0.00412	0.00226
		Compression	0.00102	0.00073	0.00068
	Concepcion EQ.	Tension	0.0153	0.0243	0.0161
		Compression	0.00918	0.00134	0.00341

strain of the reinforcement, ε_y=0.002 m/m, which is consistent with the horizontal cracks of the outer wall in Fig. 20. Under the Concepcion earthquake, the maximum tensile and compressive strains are 0.0252 m/m at boundary 5 and 0.0155 m/m at boundary 3, respectively. The compressive strain is larger than the ultimate compressive strain of concrete, $\varepsilon_{c,ult}$=0.006 m/m. The buckling of the vertical reinforcement is not modeled in the analytical material model. However, a compression strain larger than 1.5% may cause not only spalling of concrete but also buckling of reinforcement (Tuna and Wallace 2014). The values of axial strain demand in the flexible-base model are generally larger than those in the fixed-base model.

9. Conclusions

The present study was undertaken to investigate the seismic performance of three-dimensional high-rise RC box-type wall building structures based on analytical simulations of shake-table responses on a 1:5 scale 10-story RC box-type wall building model (Lee *et al*. 2012b) by using the nonlinear analysis program, PERFORM-3D V5 (CSI, 2011). The following conclusions are drawn based on the analytical results:

(1) Through nonlinear time history analyses of the model, the global behaviors, such as the natural period, stiffness, strength, and deformations, of the shake-table test could be simulated reasonably well. Under DE in Korea, the maximum IDR in the experiment/analysis results is 0.307%/0.331% in the X direction and 0.252%/0.195% in the Y direction, which satisfy the allowable IDR of 1.5% imposed by KBC 2005 (IBC 2000).

(2) The experimental and analytical models possessed a large overstrength. Under MCE in Korea, the maximum base shear coefficients of the experiment/analysis are 0.206/0.17 in the X direction and 0.272/0.30 in the Y direction, respectively. These are 2.5~3.0 times larger than the design seismic coefficients, C_s, 0.072 (X-dir.) and 0.108 (Y-dir.). In the results of the static pushover analyses, the overstrength factor of the model, Ω, which is defined as the ratio of the maximum strength of the fully-yielded system to the design seismic coefficients, is 3.22 in the X direction and 4.2 in the Y direction. In the capacity curves, the lateral strength dropped suddenly after the point of the peak resistance due to the shear failure in the Y-directional outer walls. The overstrength of the model is larger than the value of the overstrength factor, 2.5, given in KBC

2005 and IBC 2000.

(3) The behavior of the analytical model is governed by the membrane action due to the coupling beams and slabs, which partially explains the large overstrength. The coupling behavior of the walls covers approximately 40~50% of the total OTM. Similar to the test result in which the outer walls have many horizontal cracks at the lower stories subjected to a large membrane force, the analysis shows that under MCE in Korea, the maximum axial strain demands of the wall boundaries in the lower part of the first story are 0.0012 m/m in compression and within 0.006 m/m in tension, which is larger than the yield strain of steel, 0.002 m/m. However, the probability of any damage due to the concrete spalling and reinforcement buckling is very low under MCE in Korea, in contrast to the case of the 2010 Concepcion, Chile earthquake.

(4) Analytical models that neglect the flexibility of foundations and the flexural rigidity of the slabs have been widely used by engineers in practice to analyze this type of building structures. In this study, it was shown that the fixed-base condition increases the initial stiffness by 94% and 240% in the X and Y directions, respectively, with shortened fundamental periods, and decreases the lateral drift by 41% and 62% in the X and Y directions, respectively, under MCE in Korea. The ratio of the amounts of dissipated energy in the wall : slab : coupling beam in the flexible-base model is approximately 7:2:1, whereas that in the fixed-base model is about 8:1.2:0.8, which indicates that the fixed-base model increases the dissipated inelastic energy in the wall while decreasing those in the slab and coupling beam under MCE in Korea. In the model that does not include the slabs as lateral resisting elements, the initial stiffness and maximum strength are reduced to approximately half those of the model with slab. The slab increases the tension and compression coupling actions resulting in a large membrane force of the wall, and the strength of the model with slab is 25~35% larger than that without slabs. Therefore, the analytical model of the RC box-type wall building structure, which neglects the flexibility of foundations and the flexural rigidity of the slabs, should be avoided for a reliable seismic design.

(5) During the 2010 Concepcion, Chile earthquake (M_w 8.8), the main observed damage to slender walls was concrete spalling in unconfined elements and buckling and fracture of the reinforcement. Although a strong earthquake such as the 2010 Concepcion earthquake in Chile is considered unlikely to occur in low-to-moderate seismicity regions such as Korea, this study investigates the seismic performance of the model under the long-duration strong earthquake ground motion recorded in the Concepcion earthquake. Under this earthquake with three components of ground motions, the total dissipated energy is approximately 10 times larger than that under MCE in Korea. The maximum tensile and compressive strains, 0.0252 m/m and 0.0154 m/m, respectively, occurred at the wall boundaries, which indicates a potential for severe damage due to the concrete spalling and reinforcement buckling at the walls. The influence of the vertical component of ground motions appears to be negligible.

Acknowledgments

The research presented herein was supported by the Natural Hazard Mitigation Research Group, Ministry of Public Safety and Security of Korea, through the contract No. MPSS-NH-2013-70. The authors are grateful for this support.

References

ASCE (2006), *Minimum Design Loads for Buildings and Other Structures, ASCE/SEI 7-05*, American Society of Civil Engineers, Reston, VA.
ASCE (2014), *Seismic Evaluation and Retrofit of Existing Buildings, ASCE/SEI 41-13*, American Society of Civil Engineers, Reston, VA.
ACI (1995), *Building Code Requirements for Structural Concrete, ACI 318-95*, American Concrete Institute, Farmington Hills, MI.
AIK (2001), *AIK 2000*, Architectural Institute of Korea, Seoul, Korea. (in Korean)
AIK (2005), *Korean Building Code, KBC 2005*, Architectural Institute of Korea, Seoul, Korea. (in Korean)
Balkaya, C. and Kalkan, E. (2003), "Estimation of fundamental periods of shear-wall dominant building structures", *Earthq. Eng. Struct. Dyn.*, **32**(7), 985-998.
Balkaya, C. and Kalkan, E. (2004), "Seismic vulnerability, behavior and design of tunnel form building structures", *Eng. Struct.*, **26**(14), 2081-2099.
Boroschek, R., Soto, P. and Leon, R. (2010), *Maule Region Earthquake February 27, 2010, M_w=8.8*, Renadic Report 10/08 Rev.2, University of Chile, Santiago, Chile.
CSA. (2004), *Design of concrete structures, CSA A23.3-04*. Canadian Standards Association, Rexdale, Ontario, Canada.
CSI (2011), *Components and Elements for PERFORM 3D and PERFORM-Collapse Ver. 5*, Computers and Structures Inc., Berkeley, CA.
ICC (2000), *International Building Code, IBC 2000*, International Code Council, Country Club Hills, IL.
Kalkan, E. and Yüksel, S.B. (2008), "Pros and cons of multistory RC tunnel-form (box-type) buildings", *Struct. Des. Tall Spec. Build.*, **17**(3), 601-617.
Kam, W.Y., Pampanin, S. and Elwood, K. (2011), "Seismic performance of reinforced concrete buildings in the 22 February Christchurch (Lyttelton) earthquake", *Bull. NZ. Soc. Earthq. Eng.*, **44**(4), 239-278.
Korea National Statistical Office (KNSO) (2010), *Population and Housing Census*. (in Korean)
Kunnath, S.K., Panahshahi, N. and Reinhorn, A.M. (1991), "Seismic response of RC buildings with inelastic floor diaphragms", *J. Struct. Eng.*, **117**(4), 1218-1237.
Lee, D.G., Kim, H.S. and Hah, C.M. (2002), "Efficient seismic analysis of high-rise building structures with the effects of floor slabs", *Eng. Struct.*, **24**(5), 613-623.
Lee, H.S. and Woo, S.W. (2002), "Effect of masonry infills on seismic performance of a 3-storey R/C frame with non-seismic detailing", *Earthq. Eng. Struct. Dyn.*, **31**(2), 353-378.
Lee, H.S., Lee, J.J. and Jung, D.W. (2008), "Analytical simulation of shake-table responses of a torsionally-eccentric piloti-type high-rise RC building model", *Proceedings of the 14th World Conference on Earthquake Engineering*, Beijing, China.
Lee, H.S., Jeong, D.H. and Hwang, K.R. (2012a), "Analytical simulation of reversed cyclic lateral behaviors of an RC shear wall sub-assemblage", *Comput. Concrete*, **10**(2), 173-196.
Lee, H.S., Hwang, S.J., Lee, K.B., Kang, C.B., Lee, S.H. and Oh, S.H. (2012b), "Earthquake Simulation Tests on a 1:5 Scale 10-Story RC Residential Building Model", *Proceedings of the 15th World Conference on Earthquake Engineering*. Lisbon, Portugal.
Massone, L.M., Bonelli, P., Lagos, R., Lüders, C., Moehle, J. and Wallace, J.W. (2012), "Seismic design and construction practices for RC structural wall buildings", *Earthq. Spectra*, **28**(S1), S245-S256.
Moehle, J.P., Acevedo, C. and Creagh, A. (2010), "Exploratory tests of wall boundary elements subjected to alternating tensile and compressive loadings", *Poster and oral presentations at 2010 PEER Annual Meeting*.
NIST (2012), *Soil-Structure Interaction for Building Structures*, GCR 12-917-21, prepared by the NEHRP Consultants Joint Venture, a partnership of the Applied Technology Council and the Consortium of Universities for Research in Earthquake Engineering, for National Institute of Standards and Technology (NIST), Gaithersburg, Maryland.
Panagiotou, M., Restrepo, J.I. and Conte, J.P. (2010), "Shake-table test of a full-scale 7-story building slice. Phase I: Rectangular wall", *J. Struct. Eng.*, **137**(6), 691-704.
Tuna, Z. and Wallace, J.W. (2014), "Collapse Assessment of the Alto Rio Building in the 2010 Chile Earthquake", *Earthq. Spectra*, In-Press (Published Online: April 15, 2014).

Yuksel, S.B. and Kalkan, E. (2007), "Behavior of tunnel form buildings under quasi-static cyclic lateral loading", *Struct. Eng. Mech*., **27**(1), 99-115.
Wallace, J.W. (2010), "Performance-based design of tall reinforced concrete core wall buildings", *Earthquake Engineering in Europe*, 279-307, Springer, Netherlands.
Wallace, J.W., Massone, L.M., Bonelli, P., Dragovich, J., Lagos, R., Lüders, C. and Moehle, J. (2012), "Damage and implications for seismic design of RC structural wall buildings", *Earthq. Spectra*, **28**(S1), S281-S299.

KT